Linear Wave-Vector Shifts in the Raman Spectrum of α-Quartz and Infrared Optical Activity*

A. S. PINE AND G. DRESSELHAUS
Lincoln Laboratory, Massachusetts Institute of Technology, Lexington, Massachusetts 02173
(Received 7 July 1969)

Fine structure has been observed in the low-temperature Raman spectrum of the 128-cm^{-1} E mode in α-quartz. This structure is a manifestation of an allowed linear dependence of the optical-phonon frequency on wave vector. Since Raman scattering probes a small but finite wave vector, it is possible to observe these frequency shifts using high-resolution thermal or simulated Raman spectroscopy. The linear splitting of the 128-cm^{-1} E-mode doublet is $0.86\pm0.05\times10^5$ cm/sec as determined by backscattering with several laser wavelengths. Such linear wave-vector shifts lead to optical activity in the far infrared (IR). The theory of the strength and dispersion of infrared rotary power is developed in order to establish the connection between the two phenomena. The rotary power for the 128-cm^{-1} resonance can be estimated from the measured linear shift, lifetime, and IR oscillator strength. However, a direct IR rotation measurement would be hindered by the associated absorption.

INTRODUCTION

USING Raman scattering, we have measured for the first time a linear wave-vector dependence of the frequency of a zone-center optical phonon. The observation was made on the low-temperature 128-cm^{-1} E mode in α-quartz. This mode is doubly degenerate at $\mathbf{q}=0$, but the degeneracy is lifted to first order in wave vector along the c axis. Since Raman scattering probes a small but finite wave vector, by using high-resolution thermal or stimulated Raman spectroscopy, it is possible to observe a splitting. In the usual case, where linear terms are not present, typical Raman shifts that are due to parabolic dispersion would be less than 10^{-3} cm^{-1}, and so would not be resolvable. The shifts measured here are two orders of magnitude larger, and are resolved from the very narrow natural linewidth of the 128-cm^{-1} mode at liquid-helium temperature.[1]

The 128-cm^{-1} E mode is also infrared- (IR-)active. The effect of the linear wave-vector shift on the coupled photon modes is manifest as a resonant dispersion in the IR optical activity. The connection between linear wave-vector shifts and optical activity is not accidental. Similar symmetry considerations apply to the two phenomena since optical rotary power can be viewed as arising from linear terms in a wave-vector expansion of the dielectric tensor. This connection was also noted by Portigal and Burstein[2] in discussing the related problem of acoustical activity. A general theory of IR rotary power is presented in the Appendix. It is demonstrated that the linear shifts are the predominant cause of optical activity near a lattice resonance. The rotation for the 76 μ mode in α-quartz is calculated from the measured oscillator strength, linewidth, and linear shift.

Observation of linear wave-vector shifts for IR-active phonons may be complicated experimentally by two effects. The first is the additional wave-vector dependence of the frequency in the polariton regime.[3] This regime may be studied by near-forward Raman scattering, or avoided by large-angle scattering. The second complication arises in noncubic crystals, where the longitudinal-transverse character of a mode varies anisotropically.[4] Thus, LO-TO shifts may occur with the direction of the wave vector. However, the IR coupling is so weak for the 128-cm^{-1} E mode in α-quartz that the LO-TO splitting is unresolvable. A slight misorientation of $\mathbf{q}$ from the c axis therefore will not noticeably affect the measurement.

THEORETICAL CONSIDERATIONS

There are two aspects to a theory of linear wave-vector shifts in the phonon spectra of crystals. The first is the general symmetry requirements that permit such a dispersion; the second is an estimate of the magnitude of the effect. Group-theoretical considerations yield the possible crystal classes, phonon symmetries, and wave-vector orientations that may exhibit linear shifts. A cursory description of these considerations is presented in this section, and a more detailed analysis, using quartz as an illustrative example, is given in the Appendix. The magnitude of the linear shift depends, in principle, on the solution of some lattice-dynamical model such as the Born–von Karman central-force model.[5] However, for quartz it is possible to give an *ad hoc* symmetry argument for the approximate splitting of the mode under study. This argument is emphasized because of its simplicity and its applicability to several other interesting crystals. It is not intended to be highly accurate or completely generalizable to all other materials that show linear phonon dispersion.

We now examine the circumstances under which linear shifts are allowed for zone-center phonons. Many of the concepts here have their counterpart in the

* Work sponsored by the U. S. Air Force.
[1] A. S. Pine and P. E. Tannenwald, Phys. Rev. **178**, 1424 (1969).
[2] D. L. Portigal and E. Burstein, Phys. Rev. **170**, 673 (1968).
[3] J. F. Scott, L. E. Cheesman, and S. P. S. Porto, Phys. Rev. **162**, 834 (1967).
[4] R. Loudon, in *Light Scattering Spectra of Solids*, edited by G. B. Wright (Springer-Verlag, New York, 1969), p. 25.
[5] M. M. Elcombe, Proc. Phys. Soc. (London) **91**, 947 (1967).

analogous problem for electronic bands.[6] The results are not identical, however, because the absence of spin restricts the conditions for an allowed linear slope of the zone-center-phonon levels. In fact, we find that linear shifts for phonons may occur only (1) along the c axis for doublets in the uniaxial crystals 4, 422, 3, 32, 6, 622, and (2) isotropically for triplets in the cubic crystals 23, 432. Portigal and Burstein[2] show that these are also the crystal classes that may exhibit acoustical activity. The above crystals, modes, and axes are obtained from the following analysis.

For a given wave vector $\mathbf{q}$ there are $3N$ coupled equations of motion for the Fourier amplitudes of the N ions per unit cell. Since we are concerned only with the branches near the center of the zone, we take the basis functions to be the normal modes at $\mathbf{q}=0$, labeled by their irreducible representations Γ_i. Thus, the dynamical equations-of-motion matrix is diagonal at $\mathbf{q}=0$, with eigenvalues $\omega^2=\omega_{\Gamma_i}^2$. At finite $\mathbf{q}$, the matrix may be expanded as a Taylor series in wave vector, and the new normal modes will be linear combinations of the Γ-point modes, aside from the phase $e^{i\mathbf{q}\cdot\mathbf{r}}$.

It is convenient to subdivide the dynamical matrix into an $N\times N$ array of 3×3 submatrices. The 3×3 submatrix is sufficient to contain the highest possible phonon degeneracy. Any arbitrary 3×3 matrix can be formed from a basis of nine linearly independent matrices such as J^0, J_x, J_y, J_z, J_x^2, J_y^2, $J_xJ_y+J_yJ_x$, $J_yJ_z+J_zJ_y$, and $J_zJ_x+J_xJ_z$.[7] These matrices are representations of the angular-momentum operator $\mathbf{J}=\mathbf{r}\times\mathbf{p}$ for $J=1$, where

$$J^0=\begin{pmatrix}1&0&0\\0&1&0\\0&0&1\end{pmatrix},\quad J_x=\begin{pmatrix}0&0&0\\0&0&-i\\0&i&0\end{pmatrix},$$

$$J_y=\begin{pmatrix}0&0&i\\0&0&0\\-i&0&0\end{pmatrix},\quad J_z=\begin{pmatrix}0&-i&0\\i&0&0\\0&0&0\end{pmatrix}.$$

Such matrices satisfy the usual rules $J_x^2+J_y^2+J_z^2=J^0(J^0+1)$, and $\mathbf{J}\times\mathbf{J}=i\mathbf{J}$. This basis is not unique, but is chosen for its symmetry-transformation properties.

The equations of motion, and hence also the dynamical matrix, must be invariant under time reversal and the symmetry operations of the crystal. The latter invariance is assured if the Taylor series expansion of the dynamical matrix is constructed from Γ_1 (scalar) symmetry combinations of the above basis submatrices with the various powers of $\mathbf{q}$. Furthermore, under time inversion both $\mathbf{q}$ and $\mathbf{J}$ change signs, so that the odd powers of $\mathbf{q}$ can combine only with the linear J_i matrices, whereas the even powers of $\mathbf{q}$ combine only with J^0 or J_iJ_j components. Therefore, matrix elements can be linear in $\mathbf{q}$ if and only if some of the vector components q_i transform according to the same irreducible representations as J_j; that is, $\Gamma_{q_i}\times\Gamma_{J_j}$ must contain Γ_1. For example, this eliminates all crystals with a center of symmetry, since $\mathbf{q}$ is odd under space inversion while $\mathbf{J}$ is even.

Of the linear $\mathbf{q}$ matrix elements that may exist because $\Gamma_q\times\Gamma_J$ contains Γ_1, those which couple a phonon mode of Γ_k symmetry to one of Γ_j will vanish unless $\Gamma_{q_i}\times\Gamma_j$ contains Γ_k. For example, the doublet E modes in the cubic system can only couple to the triplet T modes, since $T_{q_i}\times E=T_j+T_k$.[8] In addition, as shown by a simple example in the Appendix, those matrix elements that couple levels that are nondegenerate at $\mathbf{q}=0$ can only contribute quadratically to the eigenvalue shift. Conversely, degenerate levels coupled by a matrix element are split linearly. A corollary of this condition is that no singlets may show a linear $\mathbf{q}$ shift. Therefore, it is clear that triclinic, monoclinic, and orthorhombic crystals cannot show the effect, since their symmetry is too low to have phonon representations higher than one-dimensional.

From this set of rules we may establish the criteria of crystal class, phonon mode, and wave-vector direction given at the outset. Some of these rules may be stated in a more transparent, if less rigorous, way by analogy with electronic energy levels. For example, time reversal requires the frequency of a singlet to be equal at $\pm\mathbf{q}$. Similarly, space inversion requires the same, even for a level within a degenerate manifold. This evenness precludes the possibility of linear $\mathbf{q}$ shifts.

To this point the discussion has treated the ionic system as isolated from external forces such as may arise from electron-phonon interaction, or coupling to the electromagnetic field. The former interaction has been considered for cubic covalent crystals.[9] Electromagnetic coupling is particularly important near the zone center for IR-active modes in ionic crystals. Its inclusion in this problem makes the connection between linear $\mathbf{q}$ shifts and optical activity as mentioned in the Introduction. This is readily demonstrated by the example in the Appendix. We derive there the dispersion of the rotary power near the IR resonance.

The magnitude of the linear wave-vector splitting of the 128-cm^{-1} E mode in α-quartz can be estimated from an *ad hoc* argument that is based on the simplified phonon-dispersion model in Fig. 1. The zeroth approximation for obtaining optical-phonon branches with a multiatomic unit cell is to fold back the large-zone acoustic branch of a monatomic cell. We have triply segmented a sinusoidal curve on the right to correspond to the three molecules per unit cell in α-quartz. Usually at the reciprocal-lattice vectors $\boldsymbol{\kappa}$, corresponding to twice the Brillouin-zone boundaries, the structure factors $S(\boldsymbol{\kappa})=\sum_\mu f_\mu e^{i\boldsymbol{\kappa}\cdot\boldsymbol{\tau}_\mu}$ are nonzero.

[6] C. Kittel, *Quantum Theory of Solids* (John Wiley & Sons, Inc., New York, 1963), Chap. 14 and references therein.
[7] J. M. Luttinger, Phys. Rev. **102**, 1030 (1956).
[8] G. F. Koster, J. O. Dimmock, R. G. Wheeler, and H. Statz, *Properties of the Thirty-Two Point Groups* (The MIT Press, Cambridge, Mass., 1963).
[9] G. Dresselhaus and M. S. Dresselhaus, Intern. J. Quantum Chem. **IIS**, 333 (1968).

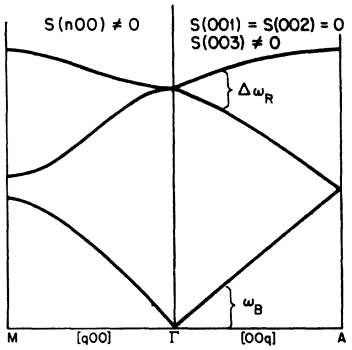

FIG. 1. Simplified phonon-dispersion model: folded zone scheme.

Here f_μ is the form factor of atom μ located with position vector τ_μ in the unit cell. $S(\kappa)\neq 0$ is the condition for Bragg reflection of a wave; for example, x rays are diffracted at such a reciprocal-lattice point. Such a reflection implies zero group velocity of the phonon or, equivalently, a horizontal dispersion curve at the zone boundaries, as illustrated on the left-hand side of Fig. 1. Along the trigonal screw axis in α-quartz, however, the structure factors associated with the $\langle 001\rangle$ and $\langle 002\rangle$ reciprocal-lattice vectors vanish. Hence, there is no Bragg reflection and the dispersion curves approach the zone edges with a finite slope. Interestingly, for the folded sinusoid along the c axis, the frequency splitting of the Raman doublet $\Delta\omega_R$ is equal to the Brillouin shift ω_B at the same small wave vector. ω_B is typically on the order of 1 cm^{-1}.

In the real crystal, the lattice dispersion is considerably modified because other modes interact with those of the simple model. This is apparent in Fig. 2, where we show the actual dispersion in α-quartz along the c axis as measured by neutron spectroscopy.[5] The principal distortion of the simple model occurs from the anticrossing of the Δ_2 modes. This mutual repulsion reduces the linear splitting of the 128-cm^{-1} mode from that of the sinusoidal case, but the neutron data are too coarse to obtain an accurate estimate for this splitting. Obviously all the E modes in α-quartz may show linear dispersion near the zone center because of the vanishing $\langle 002\rangle$ structure factor.

Similarly all (and only) crystals with a primitive three- four- or sixfold screw axis have a vanishing structure factor associated with the zone center in the folded scheme.[10] These crystals are a subgroup of those symmetry classes that permit linear $\mathbf{q}$ shifts, so they may have a dispersion comparable to α-quartz. Examples are Se, Te, HgS, and β-quartz, which all have threefold screw axes; the first three have the same space group as α-quartz ($P3_121$). $NiSO_4\cdot 6H_2O$ ($P4_12_12$) has a fourfold screw axis. A prominent example of a crystal without such a screw axis, but within the linear shift category, is $NaClO_3$ ($P2_13$).

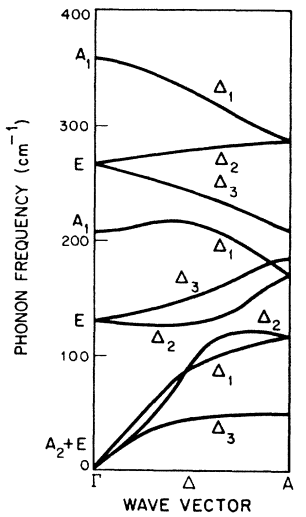

FIG. 2. Dispersion of lower-energy phonons along trigonal axis in α-quartz. After Elcombe (Ref. 5).

EXPERIMENT

In Fig. 3 we show some of the experimental traces obtained by backscattering along the c axis in α-quartz with a single-mode Ar^+ laser at 4880 Å. Backscattering gives the largest splitting, since the shift is linearly dependent on the wave-vector transfer to the phonon. The filtered 128-cm^{-1} Raman light is analyzed in a pressure-scanned Fabry-Perot interferometer with a free spectral range of 2.60 cm^{-1}. The laser light that leaks through the filters acts as a marker. The upper trace corresponds to linearly polarized incident light that is scattered by both branches of the E-mode phonon, giving rise to a Raman doublet. The two normal modes are circularly polarized in opposite direc-

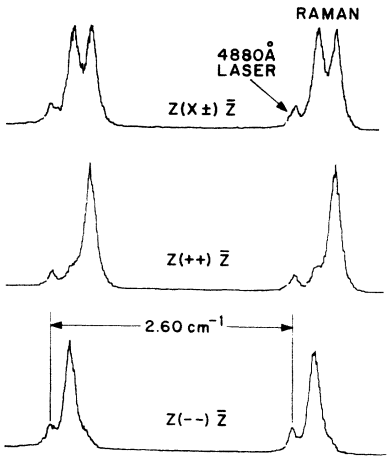

FIG. 3. High-resolution Raman scattering from 128-cm^{-1} E mode in α-quartz at 5°K. Backscattering of 4880-Å light along c axis; Fabry-Perot analyzer with free spectral range 2.60 cm^{-1}. Upper trace, linear polarization; lower traces, opposite circular polarizations.

[10] *International Tables for X-ray Crystallography* (Kynoch Press, Birmingham, England, 1952), Vol. I, Sec. 4.7.

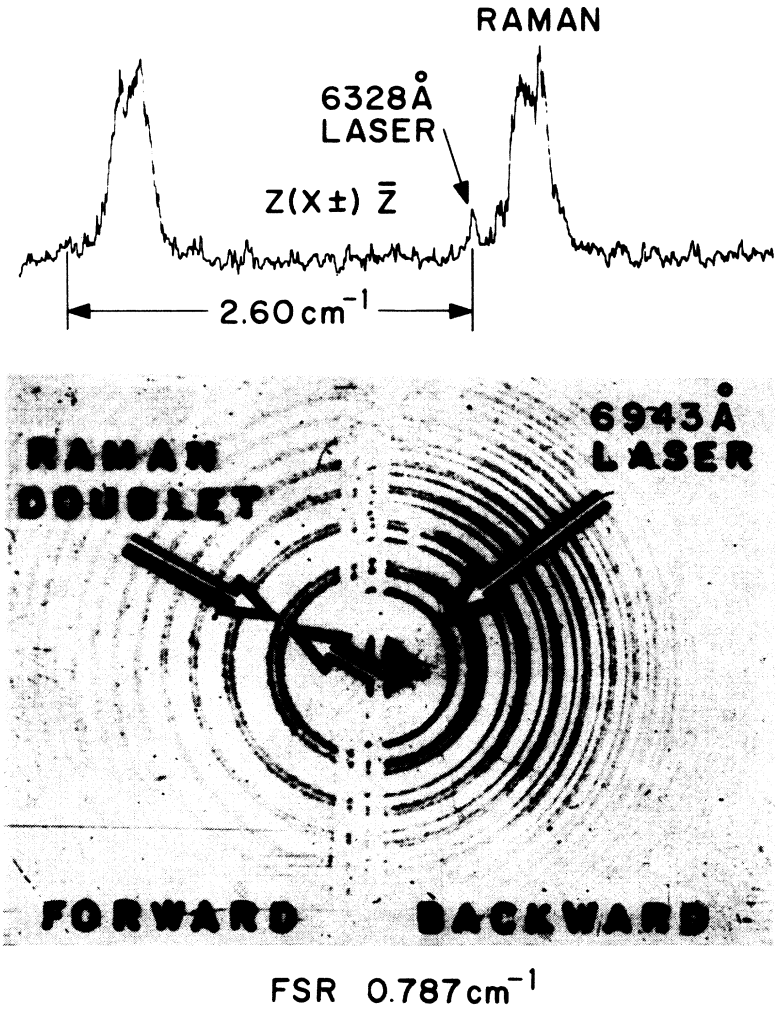

FIG. 4. High-resolution Raman scattering from 128-cm^{-1} E mode in α-quartz along c axis at 5°K. Upper trace, backscattering of 6328-Å light, FSR 2.60 cm^{-1}, linear polarization. Lower interferogram, stimulated backscattering of 6943-Å light, FSR 0.787 cm^{-1}, linear polarization.

tions, as seen in the Appendix. In an IR absorption measurement, this would be manifest as circular dichroism or, concomitantly, rotary power dispersion. The use of circularly polarized laser light discriminates between the two normal modes, as seen in the lower traces. The measured left-right splitting for this experimental geometry and wavelength is 0.19±0.01 cm^{-1}.

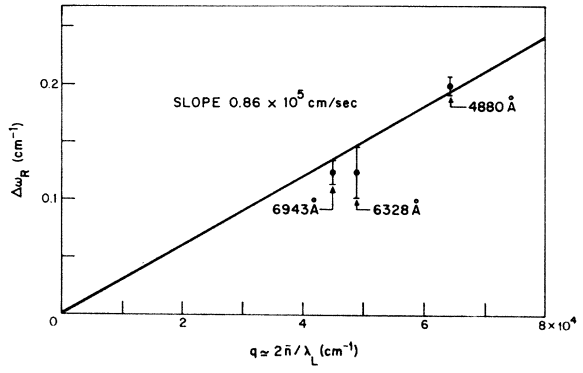

FIG. 5. Raman doublet splitting for 128-cm^{-1} E mode in α-quartz.

In Fig. 4 we again show the doublet obtained with a He-Ne 6328-Å laser and a Q-switched ruby laser at 6943 Å. For these smaller wave vectors, the doublet splitting is barely resolvable from the very narrow natural linewidths. The resolution is improved, however, by using stimulated scattering, which greatly emphasizes the peaks of the spectrum. The free spectral range of the upper trace is again 2.60 cm^{-1}; and, for the lower interferogram, it is 0.787 cm^{-1}. Forward scattering is observed in the interferogram because of reflections from the rear face of the crystal. All measurements are taken at helium temperature to sharpen the spectra.[1]

A graph of the Raman doublet splitting versus wave vector, for our three laser frequencies, is shown in Fig. 5. The linear splitting in velocity units is 0.86±0.05×10^5 cm/sec, which is about 1/7 the velocity of longitudinal sound along the c axis in α-quartz. Recall that the simple approximation in Fig. 1 would have the doublet

splitting equal to the velocity of sound. From the standpoint of a lattice dynamics, accurate measurement of such linear terms in the phonon dispersion complements neutron scattering data in much the same way as a sound-velocity measurement would.

The E doublet may also be split anisotropically by electrostatic forces for propagation directions off the c axis. With a small misorientation, such anisotropy could mask the linear wave-vector effect if the LO-TO splitting in the basal plane were much greater than the TO^+-TO^- splitting along the c axis. However, it was previously shown[1] that, for the weakly IR-active 128-cm^{-1} mode, the LO-TO splitting is unresolved from the natural linewidth. Therefore the linear $\mathbf{q}$ shifts dominate the electrostatic effects and the anisotropic splitting is maximum along the c axis.

APPENDIX: THEORY OF LINEAR WAVE-VECTOR SHIFTS AND INFRARED OPTICAL ACTIVITY

In this section we derive the essential symmetry conditions for linear wave-vector shifts in the zone-center-phonon spectrum. The connection between this effect and optical activity is established. The magnitude of the linear $\mathbf{q}$ shift influences both the strength and the dispersion of the IR rotary power.

We begin with a general description of the lattice dynamics within the context of the rigid-ion model. The dynamical matrix is expanded in a Taylor series in wave vector, and only those terms contributing near the zone center are kept. Wherever possible we illustrate the proper construction of the matrix by a concrete example. Most of the interesting physical effects are contained in a model with the symmetry of α-quartz; however, we discuss other cases as well when warranted by completeness or simplicity.

The equations of motion for the vector displacement $\mathbf{u}(\sigma\tau)$ for ion τ in unit cell σ in the presence of an electric field $\mathbf{E}(\sigma\tau)$ are

$$m^\tau \frac{\partial^2 \mathbf{u}_i(\sigma\tau)}{\partial t^2} + \sum_{j\sigma'\tau'} \Phi_{ij}(\sigma\tau,\sigma'\tau')u_j(\sigma'\tau') = \sum_j e_{ij}{}^\tau E_j(\sigma\tau). \quad \text{(A1)}$$

Here m^τ is the mass and $\mathbf{e}^\tau$ the effective-charge tensor for ion τ. Φ is the elastic force between ions. Similarly, Maxwell's equations for the field that is driven by the lattice polarization are given by

$$c^2\nabla\times\nabla\times\mathbf{E}+\boldsymbol{\varepsilon}^\infty\cdot\frac{\partial^2\mathbf{E}}{\partial t^2}=-4\pi\sum_{\sigma\tau}[\mathbf{e}^\tau]^T\cdot\frac{\partial^2\mathbf{u}(\sigma\tau)}{\partial t^2}. \quad \text{(A2)}$$

$\boldsymbol{\varepsilon}^\infty$ is the dielectric tensor at frequencies high compared to the lattice modes. The field and vibration vectors are Fourier-analyzed in the usual way:

$$\begin{Bmatrix}\mathbf{u}(\sigma\tau)\\ \mathbf{E}(\sigma\tau)\end{Bmatrix}=\sum_q\begin{Bmatrix}\mathbf{U}_\tau\\ \mathbf{E}\end{Bmatrix}e^{i[\mathbf{q}\cdot\mathbf{r}(\sigma\tau)-\omega t]}, \quad \text{(A3)}$$

where $\mathbf{r}(\sigma\tau)$ is the equilibrium position vector of an ion at $\sigma\tau$. We make use of the periodicity of the lattice and ignore local field variations over the dimensions of the unit cell. The equations of motion for the Fourier amplitudes can now be written in matrix form

$$[\mathbf{D}(\mathbf{q})-\omega^2\mathbf{1}][\mathbf{U}]=[\mathbf{e}(\mathbf{q})/m][\mathbf{E}], \quad \text{(A4a)}$$

$$[\mathbf{F}(\mathbf{q})-\omega^2\boldsymbol{\varepsilon}^\infty(\mathbf{q})][\mathbf{E}]=[4\pi N_\sigma\omega^2\mathbf{e}(\mathbf{q})]^T[\mathbf{U}], \quad \text{(A4b)}$$

with N_σ being the number of unit cells per unit volume. $\mathbf{D}(\mathbf{q})$ is the $3N\times3N$ dynamical matrix with elements given by

$$D_{ij}{}^{\tau\tau'}(\mathbf{q})=\frac{1}{m^\tau}\sum_{\sigma'}\Phi_{ij}(\sigma\tau,\sigma'\tau')e^{i\mathbf{q}\cdot[\mathbf{r}(\sigma'\tau')-\mathbf{r}(\sigma\tau)]}. \quad \text{(A5)}$$

The 3×3 tensor $\mathbf{F}(\mathbf{q})$ is formed from the double cross product

$$F_{ij}(\mathbf{q})=c^2(q^2\delta_{ij}-q_iq_j). \quad \text{(A6)}$$

The effective-charge matrix elements $e_{ij}{}^\tau/m^\tau$ comprise a $3N\times3$ array.

The dispersion relations for the coupled phonon-photon modes are obtained from the secular determinant

$$\begin{vmatrix}[\mathbf{D}(\mathbf{q})-\omega^2\mathbf{1}] & -[\mathbf{e}(\mathbf{q})/m]\\ -[4\pi N_\sigma\omega^2\mathbf{e}(\mathbf{q})]^T & [\mathbf{F}(\mathbf{q})-\omega^2\boldsymbol{\varepsilon}^\infty(\mathbf{q})]\end{vmatrix}=0. \quad \text{(A7)}$$

This determinant may be written as generalized Lyddane-Sachs-Teller (LST) relations by eliminating $\mathbf{U}$ or $\mathbf{E}$ in Eq. (A4). Then

$$|\mathbf{F}(\mathbf{q})-\omega^2\boldsymbol{\varepsilon}(\mathbf{q})|=0, \quad \text{(A8a)}$$

where

$$\boldsymbol{\varepsilon}(\mathbf{q})=\boldsymbol{\varepsilon}^\infty(\mathbf{q})+4\pi N_\sigma[\mathbf{e}(\mathbf{q})]^T\times[\mathbf{D}(\mathbf{q})-\omega^2\mathbf{1}]^{-1}[\mathbf{e}(\mathbf{q})/m], \quad \text{(A8b)}$$

or, alternatively,

$$|\mathbf{D}'(\mathbf{q})-\omega^2\mathbf{1}|=0, \quad \text{(A8c)}$$

where

$$\mathbf{D}'(\mathbf{q})=\mathbf{D}(\mathbf{q})-4\pi N_\sigma\omega^2[\mathbf{e}(\mathbf{q})/m]\times[\mathbf{F}(\mathbf{q})-\omega^2\boldsymbol{\varepsilon}^\infty(\mathbf{q})]^{-1}[\mathbf{e}(\mathbf{q})]^T. \quad \text{(A8d)}$$

The matrices $\mathbf{D}$, $\mathbf{e}$, and $\boldsymbol{\varepsilon}^\infty$ are expanded in a Taylor series in wave vector about $\mathbf{q}=0$, where we assume that the eigenvalues and normal modes are known. There the determinant $|\mathbf{D}(0)-\omega^2\mathbf{1}|=0$ has $3N$ roots $\omega_{\Gamma_i}{}^2$, which are labeled by their irreducible representations, and the dielectric tensor is diagonal along the principal axes. Then the LST relations (A8b) and (A8d) can be written to a first approximation in a commonly recognized form. For example, in the optical branches of an alkali halide, where $\mathbf{D}(0)$, $\boldsymbol{\varepsilon}^\infty(0)$,and $\mathbf{e}(0)$ are unit 3×3 matrices and m is the reduced mass, $m_1m_2/(m_1+m_2)$, of the two ions, we have from (A8b)

$$\epsilon=\epsilon^\infty+\frac{4\pi N_\sigma e^2/m}{\omega_T{}^2-\omega^2}, \quad \text{(A9a)}$$

and from (A8d), at $\mathbf{q}=0$,

$$D'(0)=\omega_T{}^2+4\pi\mathcal{N}_\sigma e^2/m\epsilon^\infty\equiv\omega_L{}^2. \quad \text{(A9b)}$$

Equations (A8c) and (A8d) are related to Kellermann's formulation of the rigid-ion model,[11] where he divides the force matrix into short-range and long-range (Coulomb) terms. The short-range forces are equivalent to $\mathbf{D}(q)$; the Coulomb matrix has the form of the second term in (A8d) for small wave vector. The full Coulomb matrix can be reproduced by taking local field effects into account, but the difference is significant to the dispersion only near the Brillouin-zone boundaries. Another lattice-dynamics theory, known as the shell model,[12] may be derived in a similar way by including electron-phonon interactions. This interaction is particularly important in materials where the electronic transitions occur at frequencies not much higher than the phonons[9]; this constitutes a breakdown of the Born-Oppenheimer or adiabatic approximation.

We now specialize the problem by considering only a 3×3 dynamical matrix interacting with the electromagnetic field. That is, we are ignoring coupling to the remaining $3N-3$ modes, but we do not lose any of the symmetry since phonons cannot have higher than threefold degeneracy. The full symmetry involved in the linear wave-vector effects can be studied by a few examples of this type. As stated in the theoretical discussion, time reversal implies that the linear $\mathbf{q}$ expansion of the matrices must transform as the angular-momentum matrices. Therefore, the most general 3×3 matrix linear in $\mathbf{q}$ may be written

$$\mathbf{M}(\mathbf{q}^1)=\begin{pmatrix} 0 & -i\sum_j\gamma_{zj}q_j & i\sum_j\gamma_{yj}q_j \\ i\sum_j\gamma_{zj}q_j & 0 & -i\sum_j\gamma_{xj}q_j \\ -i\sum_j\gamma_{yj}q_j & i\sum_j\gamma_{xj}q_j & 0 \end{pmatrix}. \quad \text{(A10)}$$

The linear expansions $\mathbf{D}(\mathbf{q}^1)$ and $\boldsymbol{\epsilon}^\infty(\mathbf{q}^1)$ are also subject to the symmetry operations of the crystal. Thus $\Gamma_{q_i}\times\Gamma_{J_j}$ must contain Γ_1, and $\Gamma_{q_i}\times\Gamma_j$ must contain Γ_k, if Γ_j and Γ_k are the symmetries of the coupled phonon modes at the Γ point. The latter condition is required by orthogonality. The first requirement states that the $\mathbf{D}(\mathbf{q}^1)$ and $\boldsymbol{\epsilon}^\infty(\mathbf{q}^1)$ matrices be constructed from invariant combinations of q_iJ_j. In Table I we list these combinations for the common crystal symmetry operations. Only those combinations that are coincident to all the symmetry operations of the crystal may be used. For example, α-quartz has operations C_3 and C_2', so that only $q_xJ_x+q_yJ_y$ and q_zJ_z are invariant. The only nonzero components allowed then in $\mathbf{M}(\mathbf{q}^1)$ are $\gamma_{xx}=\gamma_{yy}$ and γ_{zz}. Another interesting example is the wurtzite $6mm$ class, which has operations C_2, C_3, σ_d, σ_v, so that only $q_xJ_y-q_yJ_x$ is invariant. Here the nonzero components are $\gamma_{xy}=-\gamma_{yx}$.

It should be recognized that the form of the matrix $\boldsymbol{\epsilon}^\infty(\mathbf{q}^1)$ as in (A10) is very similar to that deduced for optical activity.[13] However, only the symmetric terms $\gamma_{ij}=\gamma_{ji}$ can contribute to the rotary power. Thus, crystals such as $6mm$ are nonrotary even though linear $\mathbf{q}$ tensor elements are allowed. The reason for this is simple. The antisymmetric combinations of γ_{ij} arise from components of $\mathbf{q}\times\mathbf{J}$. Under a change of handedness of the coordinate system the rotary power must change sign, whereas the polar-axial-vector cross product does not.

The remaining selection rules for linear wave-vector shifts are best illustrated by specific examples. We choose first a set of polar modes exhibiting class 32 symmetry, which consists of a doublet E mode along x and y and a singlet A_2 along z. Then, to first order in $\mathbf{q}$ we have, from our previous considerations,

$$[\mathbf{D}(\mathbf{q})-\omega^2\mathbf{1}]=\begin{pmatrix} \omega_E{}^2-\omega^2 & -i\alpha_{zz}q_z & i\alpha_{xx}q_y \\ i\alpha_{zz}q_z & \omega_E{}^2-\omega^2 & -i\alpha_{xx}q_x \\ -i\alpha_{xx}q_y & i\alpha_{xx}q_x & \omega_{A_2}{}^2-\omega^2 \end{pmatrix}. \quad \text{(A11)}$$

Since q_z transforms as A_2 and $A_2\times E=E$, and q_x, q_y transform as E and $E\times E=A_1+A_2+E$,[8] the orthogonality condition is satisfied for all the off-diagonal elements. Ignoring, for the moment, any coupling to the electromagnetic field, we examine the roots of the secular determinant of (A11). First take $q=q_z$ and $q_x=q_y=0$. Then the three eigenvalues are

$$\omega^2=\omega_{A_2}{}^2, \quad \omega^2=\omega_E{}^2\pm\alpha_{zz}q \quad \text{(A12a)}$$

and the doublet is split linearly. Next take $q=q_x$, $q_y=q_z=0$; then

$$\omega^2=\omega_E{}^2, \quad \omega^2=\tfrac{1}{2}(\omega_E{}^2+\omega_{A_2}{}^2) \pm[\tfrac{1}{4}(\omega_E{}^2-\omega_{A_2}{}^2)^2+\alpha_{xx}{}^2q^2]^{1/2}. \quad \text{(A12b)}$$

Here, if $\omega_E{}^2$ and $\omega_{A_2}{}^2$ are not accidentally degenerate, the last two modes are split quadratically in q. These demonstrations are immediately generalizable to the prior statement that nondegenerate modes are split quadratically by the coupling matrix element. This statement is actually a well-known result of nondegenerate-perturbation theory, which is recovered term by term in (A12b) by expanding the square root.

From the above reasoning, we can discount the possibility of linear shifts for singlet modes, and, thereby, for biaxial crystals. Furthermore, orthogonality rules out the doublet modes in cubic crystals, since $T_{q_i}\times E$ does not contain E. The doublets in uniaxial crystals are only split linearly by q_iJ_z combinations as is evident in (A12a). This combination exists exclusively

[11] E. W. Kellermann, Phil. Trans. Roy. Soc. London **A238**, 513 (1940).

[12] B. G. Dick and A. W. Overhauser, Phys. Rev. **112**, 90 (1958).

[13] J. P. Mathieu, in *Handbuch der Physik*, edited by S. Flügge (Springer-Verlag, Berlin, 1957), Vol. XXVIII, p. 333, a thorough review of optical activity and an extensive bibliography.

TABLE I. Invariant combinations of q_iJ_j for common symmetry operations.

Symmetry operations on polar and axial vectors	Invariant combinations
$I(q_x,q_y,q_z)=(-q_x,-q_y,-q_z)$ $I(J_x,J_y,J_z)=(J_x,J_y,J_z)$	none
$\sigma_v(q_x,q_y,q_z)=(-q_x,q_y,q_z)$ $\sigma_v(J_x,J_y,J_z)=(J_x,-J_y,-J_z)$	q_xJ_y, q_xJ_z, q_yJ_x, q_zJ_x
$\sigma_d(q_x,q_y,q_z)=(q_y,q_x,q_z)$ $\sigma_d(J_x,J_y,J_z)=(-J_y,-J_x,-J_z)$	$q_xJ_x-q_yJ_y$, $q_xJ_y-q_yJ_x$
$\sigma_h(q_x,q_y,q_z)=(q_x,q_y,-q_z)$ $\sigma_h(J_x,J_y,J_z)=(-J_x,-J_y,J_z)$	q_zJ_y, q_zJ_x, q_xJ_z, q_yJ_z
$S_4(q_x,q_y,q_z)=(q_y,-q_x,-q_z)$ $S_4(J_x,J_y,J_z)=(-J_y,J_x,J_z)$	$q_xJ_x-q_yJ_y$, $q_xJ_y+q_yJ_x$
$C_4(q_x,q_y,q_z)=(q_y,-q_x,q_z)$ $C_4(J_x,J_y,J_z)=(J_y,-J_x,J_z)$	$q_xJ_x+q_yJ_y$, $q_xJ_y-q_yJ_x$, q_zJ_z
$C_3(q_x,q_y,q_z)=(-\frac{1}{2}q_x+\frac{1}{2}\sqrt{3}q_y,-\frac{1}{2}\sqrt{3}q_x-\frac{1}{2}q_y,q_z)$ $C_3(J_x,J_y,J_z)=(-\frac{1}{2}J_x+\frac{1}{2}\sqrt{3}J_y,-\frac{1}{2}\sqrt{3}J_x-\frac{1}{2}J_y,J_z)$	$q_xJ_x+q_yJ_y$, $q_xJ_y-q_yJ_x$, q_zJ_z
$C_3'(q_x,q_y,q_z)=(q_y,q_z,q_x)$ $C_3'(J_x,J_y,J_z)=(J_y,J_z,J_x)$	$q_xJ_x+q_yJ_y+q_zJ_z$
$C_2(q_x,q_y,q_z)=(-q_x,-q_y,q_z)$ $C_2(J_x,J_y,J_z)=(-J_x,-J_y,J_z)$	q_xJ_x, q_yJ_y, q_zJ_z, q_xJ_y, q_yJ_x
$C_2'(q_x,q_y,q_z)=(q_x,-q_y,-q_z)$ $C_2'(J_x,J_y,J_z)=(J_x,-J_y,-J_z)$	q_xJ_x, q_yJ_y, q_zJ_z, q_yJ_z, q_zJ_y
$C_2''(q_x,q_y,q_z)=(q_y,q_x,-q_z)$ $C_2''(J_x,J_y,J_z)=(J_y,J_x,-J_z)$	$q_xJ_x+q_yJ_y$, q_zJ_z, $q_xJ_y+q_yJ_x$

for the classes 4, 422, 3, 32, 6, and 622, and then only as q_zJ_z. Thus, the linear shifts occur along the c axis for all the uniaxial crystals that exhibit optical activity along this axis. The other two uniaxial optically active crystals, $\bar{4}$ and $\bar{4}2m$, do not show linear phonon shifts and are nonrotary for c-axis propagation. The cubic crystals 23 and 432 have the invariant $\mathbf{q}\cdot\mathbf{J}$, which implies $\gamma_{xx}=\gamma_{yy}=\gamma_{zz}$ and assures that the linear triplet splittings, as well as the optical activity, are isotropic.

We now return to the coupled phonon-photon problem in order to establish the influence of the linearly split modes on the IR optical activity. This is accomplished in the simulated α-quartz example by introducing a nonzero effective-charge tensor of the proper symmetry to couple to the electric field modes. Noting that the fields along the principal axes E_x and E_y have E symmetry, and that E_z has A_2, by orthogonality we see that $\mathbf{e}(\mathbf{q})$ must transform as Γ_1 to couple the fields to the same symmetry vibrations. Therefore, in this case, $\mathbf{D}$, $\boldsymbol{\epsilon}^\infty$, and $\mathbf{e}$ all have the same form as (A11). As a further simplification, we take purely c-axis propagation, so $q=q_z$, $q_x=q_y=0$, and let $\alpha_{zz}=\alpha$. Each of the 3×3 submatrices is diagonalized, as indicated in (A12a), by a unitary transformation of the (x,y) polar modes to a set of circularly polarized modes $(1/\sqrt{2})(x\pm iy)$. With this basis the coupled matrices in (A7) can be written

$$\begin{vmatrix} \omega_E{}^2-\omega^2+\alpha q & 0 & 0 & -(e_E+\eta q)/m & 0 & 0 \\ 0 & \omega_E{}^2-\omega^2-\alpha q & 0 & 0 & -(e_E-\eta q)/m & 0 \\ 0 & 0 & \omega_{A_2}{}^2-\omega^2 & 0 & 0 & -e_{A_2}/m \\ -4\pi N_o\omega^2(e_E+\eta q) & 0 & 0 & c^2q^2-\omega^2(\epsilon_E{}^\infty+\beta q) & 0 & 0 \\ 0 & -4\pi N_o\omega^2(e_E-\eta q) & 0 & 0 & c^2q^2-\omega^2(\epsilon_E{}^\infty-\beta q) & 0 \\ 0 & 0 & -4\pi N_o\omega^2 e_{A_2} & 0 & 0 & -\omega^2\epsilon_{A_2}{}^\infty \end{vmatrix}=0. \quad \text{(A13)}$$

Here m is dependent on the particular combination of ionic motions making up the given normal mode. We have absorbed its index and wave-vector dependence in the effective charge.

The solutions of the secular equation (A13) are obtained from three 2×2 determinants. The dispersion of the E modes is expressed in the form of Eq. (A8b) for the phonon-modified dielectric tensor

$$\epsilon_E{}^\pm=\epsilon_E{}^\infty\pm\beta q+\frac{(4\pi N_o/m)(e_E\pm\eta q)^2}{\omega_E{}^2-\omega^2\pm\alpha q}. \quad \text{(A14)}$$

The rotary power per unit length is given by

$$\rho=\tfrac{1}{2}q\bar{n}[\sqrt{\epsilon_E{}^+}-\sqrt{\epsilon_E{}^-}]=(q/4\bar{n}^2)[\epsilon_E{}^+-\epsilon_E{}^-], \quad \text{(A15)}$$

where we can neglect the relatively small linear q terms in

$$\bar{n}=\tfrac{1}{2}[\sqrt{\epsilon_E{}^+}+\sqrt{\epsilon_E{}^-}]\simeq[\epsilon^\infty+G/(\omega_E{}^2-\omega^2)]^{1/2}, \quad \text{(A16)}$$

where $G=4\pi N_\sigma e_E{}^2/m=S_1\omega_E{}^2$, and S_1 is the oscillator strength. To first order in q

$$[\epsilon_E{}^+-\epsilon_E{}^-]=2\beta q+\frac{(4G\eta/e_E)q(\omega_E{}^2-\omega^2)-2G\alpha q}{(\omega_E{}^2-\omega^2)^2-(\alpha q)^2}. \quad \text{(A17)}$$

The rotary power then has three distinct linear q terms. β is contributed by the electronic resonances and is measurable from the usual visible optical activity. Normally βq is very small in the far IR. η arises from the dipole expansion of the effective charge and so far, has not been observed. The parameter α measures the linear frequency splitting, which we know from the Raman experiment reported here. α can be written $\omega_E v$, where v is of the order of the velocity of sound.

The dispersion of the IR rotary power consists of two peaks at $\omega_E\pm\alpha q/2\omega_E$, as seen from (A17). Inclusion of damping keeps the resonances finite. The two peaks are odd about ω_E for the η contribution and even for the α term. Among other things, this implies that certain lattice resonances can affect even the residual electronic optical activity. Again a finite damping reduces the anomaly.

In Fig. 6 we plot a typical E-mode dispersion in the polariton regime for our simulated α-quartz example. On the left is the familiar form of the dispersion, which occurs for propagation in the basal plane of quartz. The LO and TO phonons and the IR ordinary ray are easily identified. On the right, along the c axis, the normal modes of E symmetry are transverse and circularly polarized. The difference between the IR phase velocities is a measure of the IR optical activity.

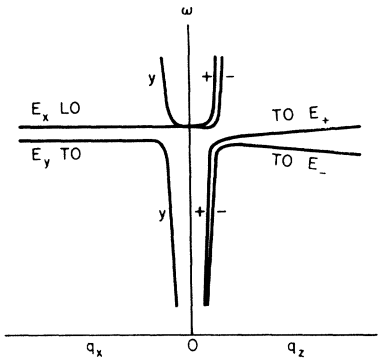

FIG. 6. Polariton dispersion relations in quartz illustrating the source of IR optical activity.

As a final example we calculate the rotary power in α-quartz for the low-temperature E-mode resonance at 76 μ. The residual electronic contribution is

$$\rho_\beta=\beta q^2/2\bar{n}^2=2\pi^2\bar{n}\beta/\lambda^2. \quad \text{(A18)}$$

From the visible rotary power[13] we have $2\pi^2\beta=1.27\ \mu^2$ rad/cm. Thus, $\rho_\beta\sim3.1\times10^{-4}$ rad/cm, which is probably unmeasurable. The doublet splitting vq is 0.8×10^{-3} cm^{-1}, where v is determined by the Raman experiment and q is the IR wave vector. Since the natural linewidth[1] $\delta\omega$ is 0.05 cm^{-1} (full width at half-maximum), the IR doublet is unresolved. Therefore, the portion ρ_η, which is due to the effective-charge expansion, is expected to be negligible near resonance, since the two overlapping modes largely cancel each other out. In the wings this expression may be significant, depending on the magnitude of η. On the other hand, the contributions due to the linear shifts are additive at resonance, so that (A17) yields

$$\rho_\alpha=\tfrac{1}{2}S_1(\omega_E/\delta\omega)(vq/\delta\omega)(q/\bar{n}^2). \quad \text{(A19)}$$

The denominator in (A17) has been written $(i\omega_E\delta\omega)^2$ in the limit, where the doublet is unresolved. An estimate of $S_1\sim10^{-4}$ at 4°K may be obtained from the room-temperature value of Russell and Bell,[14] which has been scaled according to the temperature dependence measured by Plendl *et al.*[15] With the above parameters in (A19), we obtain a substantial peak rotary power $\rho_\alpha\simeq0.9$ rad/cm. However, the concomitant IR absorption, or circular dichroism, is a serious impediment to the direct observation of the optical activity. The peak intensity absorption coefficient in the unresolved limit is, for this mode,

$$l^{-1}=S_1(\omega_E/\delta\omega)(q/\bar{n}^2)\simeq10^2\ \text{cm}^{-1}. \quad \text{(A20)}$$

Experimentally, the significant parameter is the net rotation in a damping length

$$\rho_\alpha l=\tfrac{1}{2}\bar{n}(vq/\delta\omega), \quad \text{(A21)}$$

which is independent of the oscillator strength. Thus, the 128-cm^{-1} E mode is the best candidate in α-quartz because of its relatively long lifetime. In this case, $\rho_\alpha l\simeq\frac{1}{2}$ arc degree. Portigal and Burstein[2] have suggested tellurium as a candidate for IR optical activity, though the relevant parameters have not been measured for this material. To our knowledge, there have been no observations of vibration-induced optical activity.

---

[14] E. E. Russell and E. E. Bell, J. Opt. Soc. Am. **57**, 341 (1967).
[15] J. N. Plendl, L. C. Mansur, A. Hadni, F. Brehat, P. Henry, G. Morlot, F. Naudin, and P. Strimer, J. Phys. Chem. Solids **28**, 1589 (1967).

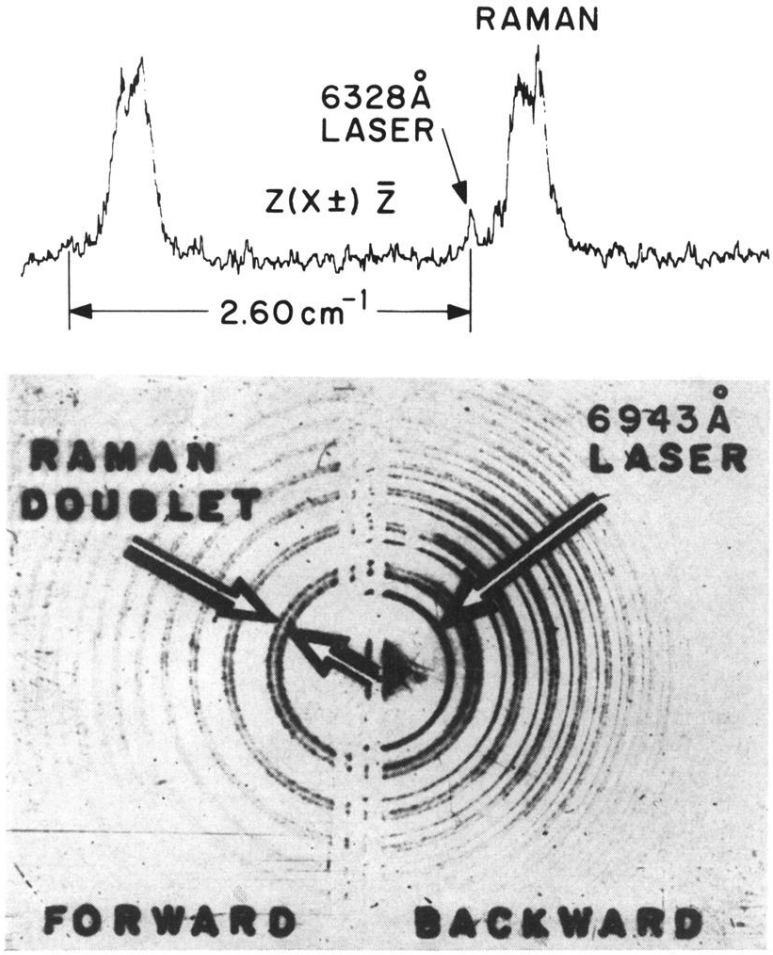

FIG. 4. High-resolution Raman scattering from 128-cm^{-1} E mode in α-quartz along c axis at 5°K. Upper trace, backscattering of 6328-Å light, FSR 2.60 cm^{-1}, linear polarization. Lower interferogram, stimulated backscattering of 6943-Å light, FSR 0.787 cm^{-1}, linear polarization.